J Mater Sci (2007) 42:8671–8689
DOI 10.1007/s10853-007-1808-2

Synthesis and characterization of carbon nanotubes grown on montmorillonite clay catalysts

Alexandra Destrée · Gary J. Long · Benjamin Vatovez · Fernande Grandjean · Antonio Fonseca · Janos B. Nagy · A.-M. Fransolet

Received: 6 March 2007 / Accepted: 26 April 2007 / Published online: 19 July 2007

Abstract Multiwall carbon nanotubes have been grown on montmorillonite clay catalysts through anchoring on FeCo nanoparticles. The starting clay is a commercial sodium-rich montmorillonite in which the intercalated sodium ion was exchanged for cobalt(II) and iron(III) ions via mechanical agitation or sonication, both with and without subsequent centrifugation. The cobalt-iron intercalate clay was used as a catalyst for the synthesis of carbon nanotubes via decomposition of ethylene at 700 °C. The largest carbon deposit was obtained for catalysts prepared with 3 or 4 cation exchange equivalents. X-ray diffraction indicates both that the basal spacing of the clay increases from 12.43 Å to 16.4 Å upon intercalation of cobalt and iron. Atomic absorption analysis of the catalysts indicates that virtually all of the sodium ions originally present in the clay have been replaced by iron(III) and cobalt(II). Transmission electron micrographs show the presence of multiwall carbon nanotubes with inner and outer diameters of ca. 10 nm and 20 nm grown on metal particles present on the plates of catalysts. The iron-57 Mössbauer spectra indicate that the intercalated clay contains iron(III) in octahedral and tetrahedral sites and iron(II) in octahedral sites, the catalysts contain an extensive amount of small superparamagnetic particles of α-Fe_2O_3 and that the carbon-nanotube catalyst composites show the presence of iron(II) and iron(III) paramagnetic doublets, characteristic of a reduced montmorillonite, and of sextets that are characteristic of an FeCo alloy and of Fe_3C cementite. The Mössbauer spectra indicate that the carbon nanotubes grow on FeCo metallic nanoparticles and bond to these particles through the formation of cementite.

A. Destrée · A. Fonseca · J. B. Nagy
Facultés Universitaires Notre-Dame de la Paix, 61, rue de Bruxelles, Namur 5000, Belgium

A. Destrée
e-mail: destree@poly.ucl.ac.be

G. J. Long
Department of Chemistry, University of Missouri-Rolla, Rolla, MO 65409-0010, USA
e-mail: glong@umr.edu

B. Vatovez · F. Grandjean (✉)
Department of Physics, University of Liège, B5, Sart-Tilman 4000, Belgium
e-mail: fgrandjean@ulg.ac.be

A.-M. Fransolet
Department of Geology, University of Liège, B18, Sart-Tilman 4000, Belgium
e-mail: amfransolet@ulg.ac.be

Introduction

The synthesis of carbon nanotubes on supported catalysts impregnated by transition metals has been achieved on various supports, such as silica [1], alumina [2], zeolites [3], and clays [4, 5]. In this work, the support is a smectite clay mineral, more specifically a sodium-rich montmorillonite, Na Cloisite®. This layered mineral, ideally $Na_x(Al_{2-x}Mg_x)(Si_4O_{10})(OH)_2 \cdot nH_2O$, consists of one octahedral sheet mainly occupied by Al^{3+} and sandwiched between two tetrahedral sheets occupied by Si^{4+}; the interlayered Na^+ maintains the charge balance of the crystal structure. Because of their unique swelling, ion exchange, and intercalation properties, smectite clays can be easily, uniformly, and reproducibly loaded with metal cations. This process is called [6] pillaring and is schematically represented in Fig. 1. In this process, the sodium cations, that are

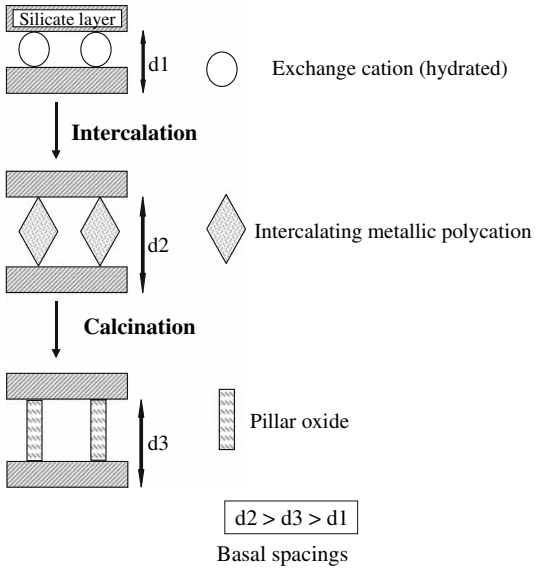

Fig. 1 A schematic representation of the pillaring process of the Na Cloisite®. Top, the initial clay, middle, the clay with intercalated iron and cobalt cations, and bottom, the clay after calcination with oxide pillars

naturally present between the layers of the clay, are replaced by transition metal cations, i.e., cobalt(II) and/or iron(III), cations that will serve as anchors [4, 5] for the growth of carbon nanotubes. Earlier work [5] has demonstrated that cobalt intercalated montmorillonite leads to better quality carbon nanotubes than does iron intercalated montmorillonite. In this work, the influence of neighboring cobalt and iron anchors on the quantity and quality of the carbon nanotubes is investigated. The long-term goal of this research is the inclusion of the carbon-nanotube clay composite into a polymer matrix to enhance some of the physical or chemical properties of the mixtures, such as their electrical and thermal conductivity and fire resistance. Herein, the synthesis of the carbon nanotubes grown on montmorillonite is reported. The results obtained by X-ray diffraction, transmission electron microscopy, thermogravimetric analysis, and iron-57 Mössbauer spectroscopy, on samples obtained at different steps in the preparative route are presented and discussed.

Preparation of catalysts and synthesis of the carbon nanotubes

A commercial sodium-rich montmorillonite, produced by Southern Clay Products Inc., with the trade name Na Cloisite®, with particle diameters of less than 13 μm, has been used as the starting material. The chemical analysis of the Na Cloisite® by a wet-chemical procedure is given in Table 1. Its cation exchange capacity is 92.6 meq/100 g of clay. The cobalt(II) and iron(III) precursors are A.C.S. reagent grade hydrated transition metal salts, $CoCl_2{\cdot}6H_2O$ and $FeCl_3{\cdot}6H_2O$, obtained from Sigma Aldrich.

Table 1 Chemical composition of the Na cloisite®

Component	Wt.%
SiO_2	55.90
Al_2O_3	19.21
Fe_2O_3	4.28
MgO	2.09
CaO	0.14
Na_2O	3.84
K_2O	0.10
TiO_2	0.11
P_2O_5	<0.01
MnO	<0.01
Cr_2O_3	<0.001
Ba	40 ppm
Ni	20 ppm
Sr	34 ppm
Zr	113 ppm
Y	17 ppm
Nb	<10 ppm
Sc	5 ppm
LOI[a]	14.3

[a] Percent weight loss on ignition

The catalysts used for the growth of the carbon nanotubes listed in Table 2 were prepared, as shown schematically in Fig. 2, by ionic exchange of the sodium

Table 2 List of catalysts and their carbon deposit, τ

Sample	τ, %	Exchange method	Centrifugation	Exchange capacity[a]
1a	0	Mechanical	No	1
1b	0	Mechanical	Yes	1
2a	0	Mechanical	No	2
2b	0	Mechanical	Yes	2
3a	83.0 ± 10.6	Mechanical	No	3
3b	48.8 ± 5.0	Mechanical	Yes	3
4a	40.3 ± 2.3	Mechanical	No	4
4b	6.1 ± 1.5	Mechanical	Yes	4
1a′	0	Sonication	No	1
1b′	0	Sonication	Yes	1
2a′	0	Sonication	No	2
2b′	0	Sonication	Yes	2
3a′	18.1 ± 3.6	Sonication	No	3
3b′	1.2 ± 0.7	Sonication	Yes	3
4a′	20.0 ± 3.3	Sonication	No	4
4b′	13.8 ± 2.5	Sonication	Yes	4

[a] One cation exchange capacity is 92.6 meq/100 g of Na Cloisite® clay

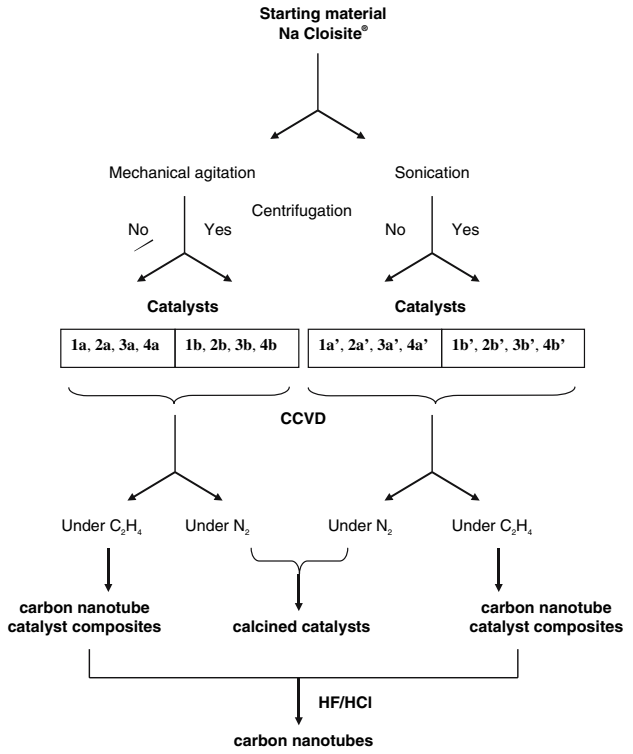

Fig. 2 A schematic of the preparative route and the labeling of the samples

in Na Cloisite®, an exchange that has been carried out in two ways. The first used mechanical agitation either without centrifugation yielding samples **1a** to **4a** or with centrifugation yielding samples **1b** to **4b**. The second used sonication either without centrifugation yielding samples **1a′** to **4a′**, or with centrifugation yielding samples **1b′** to **4b′**. Both methods used a suspension of 2 g of clay in 100 mL of water and $n \times 92.6$ meq/100 g of solutions of the transition metals, with $n =$ 1, 2, 3, and 4, for samples **1** to **4**. For samples **1a** to **4b**, the mixture is mechanically stirred for 3 h at 80 °C, allowed to settle for ca. 12 h, and dried by lyophilization for 48 h. For samples **1a′** to **4b′**, the mixture is treated in an ultrasonic bath for 1 h at room temperature, allowed to settle for ca. 12 h, and dried by lyophilization for 48 h.

The clay catalyzed synthesis of the carbon nanotubes has been carried out by the carbon vapor deposition from ethylene [7]. In this synthesis 1 g of the clay catalyst was placed in a fixed-bed reactor inside a quartz tube in which the decomposition of ethylene is carried out at 700 °C. The carrier gas was nitrogen and the reaction time was 30 min. The product of this reaction is a composite of carbon nanotubes and the clay catalyst. In the earlier work [4, 5], the carbon vapor deposition of acetylene was used for the synthesis of the carbon nanotubes. Finally, the carbon nanotubes present in the composite were removed from the clay catalyst surface by washing with concentrated hydrofluoric acid and then with concentrated hydrochloric acid at room temperature.

In order to determine the amount of water lost from the clay catalyst during the 700 °C carbon vapor deposition, a separate portion of the catalyst was calcined at 700 °C under pure nitrogen yielding the calcined catalysts shown in Fig. 2. If one assumes that the amount of water lost is the same under N_2 and ethylene as N_2 alone, then the percent fraction of the carbon deposition, τ, produced by a given clay catalyst is given by,

$$\tau = \frac{m_f - (m_i - m_{water})}{m_i - m_{water}} \times 100,$$

where m_i is the initial and m_f is the final mass of the carbon clay catalyst composite, and m_{water} is the mass of the water lost during the calcination of 1 g of the catalyst at 700 °C for 30 min under a flow of nitrogen gas. The amount of carbon deposited by the eight samples studied herein is given in Table 2.

With the mechanical agitation method, the highest carbon deposits are obtained for catalysts **3a** and **3b** containing a three cation exchange capacity of cobalt(II) and iron(III). The sonication method gives the highest carbon deposit for catalysts **4a′** and **4b′**. These results are in agreement with previous preparations [8] in which the intercalant solution used is usually in excess to ensure a high degree of saturation of the exchanged sites. Because all the other catalysts lead to negligible or small carbon deposits, our subsequent study will focus on these four catalysts.

X-ray diffraction measurements

The mineralogical nature of the Na Cloisite® was determined from its powder X-ray diffraction pattern. This pattern, see Fig. 3, obtained at room temperature with a Philips diffractometer indicates that Na Cloisite® contains a small amount of quartz and cristobalite as impurities. In addition, weak but sharp reflections at *d*-spacings of ca. 2.82, 1.99, and 2.79 Å correspond to the presence of traces of NaCl, and α-Na_2SO_4 or thenardite. The montmorillonite identification, confirmed by the basal spacing, d_{001}, at 12.43 Å, is also confirmed by the chemical composition of Na Cloisite® supplied by the manufacturer and given in Table 1. Through a comparison of the data in Table 1 and the chemical results reported in the literature [9], it seems reasonable to assume that Na Cloisite® contains between ca. 5 and 10 weight percent of impurities. The composition of the Na Cloisite® is very similar to that of the Zenith-N used in a previous study [10] of carbon nanotubes grown on montmorillonite.

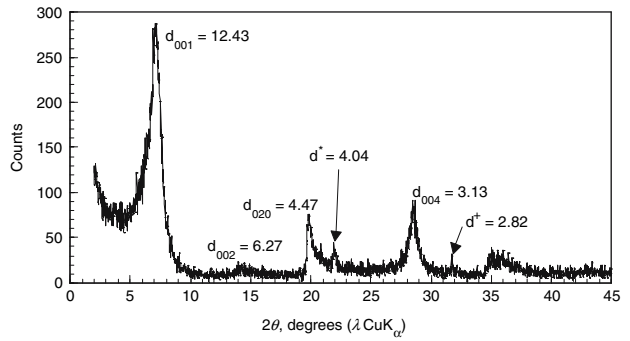

Fig. 3 The X-ray powder diffraction pattern of the Na Cloisite®. Lattice distances are indicated in Å. The * and + correspond to the most intense reflections of crystabolite and NaCl, respectively

Additional X-ray diffraction measurements of the Na Cloisite® were carried out in order to determine the swelling clay fraction. A suspension of one to two grams of the bulk Na Cloisite® in distilled water was allowed to settle for 50 min, decanted and then centrifuged at 3,000 rpm. The precipitated fraction, with a particle size of less than 2 μm as determined by Stoke's law, was used to prepare air-dried oriented aggregates [11] deposited on a glass microscope slide. A standard X-ray diffraction analysis of a clay fraction includes [12] the sequential collection of the X-ray diffraction patterns of the natural oriented air-dried aggregates, of the aggregates solvated with ethylene-glycol for 24 h, and of the aggregates after heating at 500 °C for 4 h. The first pattern reveals a basal spacing of 12.44 Å in the Na Cloisite®, a value in good agreement with the 12.43 Å value found in Fig. 3. The second pattern indicates both that the montmorillonite has expanded after solvation with ethylene glycol and that its basal spacing has increased to 16.95 Å. The third pattern indicates that after heating at 500°C for 4 h the basal spacing has decreased to 9.66 Å. The swelling behavior and the X-ray diffraction results obtained for Na Cloisite® are similar to those reported [10] for the Zenith-N.

Powder X-ray diffraction has also been used to identify the phases obtained after the different treatments of the samples shown in Fig. 2. The patterns obtained for catalysts **3a**, **4a′** and **4b′** systematically show both that the Na Cloisite® is affected by solvation, which results in an increase in its d_{001} spacing of up to ca. 16.4 Å, and that the clay is accompanied by NaCl and $CoCl_2.2H_2O$. The pattern obtained for catalyst **3b** reveals that the Na Cloisite® is relatively pure and only slightly modified to have a d_{001} spacing of ca. 13.4 Å.

The X-ray powder patterns of the calcined catalysts can be subdivided into two groups. First, the patterns obtained for **3a** and **4a′** clearly show the presence of α-Fe_2O_3, hematite, and of another oxide with a spinel-type structure. The reliability of the *d*-spacing measurements prevents a clear distinction between $Fe^{2+}Fe^{3+}{}_2O_4$ and $Co^{2+}Fe^{3+}{}_2O_4$. Moreover, the Na Cloisite® is transformed into a sodium-rich mica-like phase with a d_{001} spacing of ca. 9.6 Å to 9.8 Å. The presence of NaCl has been detected in sample **3a**. Second, the patterns obtained for **3b** and **4b′** show the presence of the clay mineral with a d_{001} spacing of ca. 9.7 Å. Finally, the modified Na Cloisite® with a d_{001} spacing of 9.7 Å is always accompanied by both a small amount of cristobalite and a spinel-like oxide similar to that found in the **3a** and **3b** catalyst composites. However, Mössbauer spectral results to be discussed below, indicate that in these composites there is little if any iron in the spinel. Sample **3b** also contains traces of NaCl.

Atomic absorption analysis

Wet-chemical measurements have been carried out with a Analytikjena Nova300 atomic absorption spectrometer. The results shown in Table 3 have been obtained after dissolution of the catalysts in a 1:1 mixture of hydrofluoric acid and hydrochloric acid. The upper half of this table gives the iron(III), cobalt(II), and sodium(I) contents in the starting mixtures of clay and transition metal salts and the lower half gives the results for the catalysts. The values given for iron(III) have been corrected for the percentage of iron(III) naturally present in the clay. The results indicate both that virtually all of the sodium ions present in the interlayer and most of the cobalt(II) has been removed from the clay by the washing treatment applied to **3b** and **4b′**, and that the total amount of transition metal ions is smaller in **3b** and **4b′** than in **3a** and **4a′**. This smaller amount seems to lead to a reduced carbon deposit as is indicated by the τ values given in Table 2. Among the four catalysts listed in Table 3, catalyst **3a**, which has the highest cobalt content, also exhibits the largest carbon deposit, whereas catalyst **4b′**, that has the lowest transition metal ion content, also exhibits the smallest carbon deposit.

Table 3 Weight percent metal composition in the starting clay/salt mixtures and after ionic exchange into the clay

Wt.%	3a	3b	4a′	4b′
Starting				
Fe(III)	18	18	24	24
Co(II)	18	18	24	24
Na(I)	3.8	3.8	3.8	3.8
After				
Fe(III)	3.0	4.5	2.6	2.3
Co(II)	4.0	0.2	2.6	0.3
Na(I)	1.9	0.1	0.9	0.1

Thermogravimetric analysis

The thermogravimetric analysis of the Na Cloisite® has been carried out with a NETSCH STA 409 PG analyzer. The temperature of the sample with a typical mass of 15–20 mg was increased from room temperature to 700 °C at a heating rate of 10 °C/min in a 50 mL/min flow of helium.

The results of the thermogravimetric analysis, see Fig. 4, indicate that the decomposition of Na Cloisite® proceeds in two steps. A mass decrease of ca. 10% is observed between 30 °C and 150 °C, a decrease that is associated [13] with the loss of both surface adsorbed water and the clay interlayer water. Between 150 °C and 450 °C, the mass decreases slowly and then more rapidly between 450 °C and 600 °C. The latter decrease corresponds [14] to the dehydroxylation of the Al–OH in the octahedral sheets, and coincides with the collapse of the clay structure. The residual mass at the end of the thermal treatment is 86.04%.

The results of the thermogravimetric analysis obtained for catalysts, **3a** and **3b**, and **4a′** and **4b′**, are shown in Fig. 5a and b, respectively. The catalysts show a more continuous and monotonic mass loss than does the clay. Below 150 °C the water adsorbed at the surface of the clay corresponds to 50% of the water loss. The loss of water associated with the microporous structure of the catalysts, i.e., the dehydroxylation associated with the interlayer pillars, begins at 150 °C. It is well known [15] that the stability of the pillars is related to the extent of their dehydroxylation, a process which affects the basal spacing.

For the preparations by both mechanical agitation and sonication, a significant difference is observed between the **a** and **b** catalysts. The **b** catalysts, that have been washed and centrifuged, show a higher residual mass after the thermal treatment. Hence, the washing eliminates the excess of hydrated transition metal salts, in agreement with the wet-chemical analysis and the X-ray diffraction patterns. The loss of water in the dehydroxylation step between 150 °C and 700 °C is more important for the **a** catalysts than for the **b** catalysts. Hence, in agreement with previous observations [16, 17], the washing step improves the thermal stability and the homogeneity of the product.

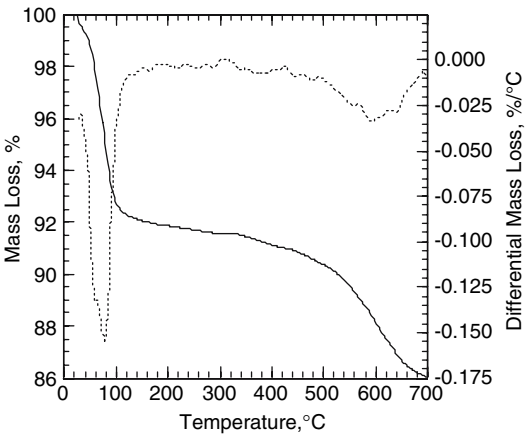

Fig. 4 The thermogravimetric analysis of the Na Cloisite®. The differential thermogravimetric analysis results are shown as the dashed line

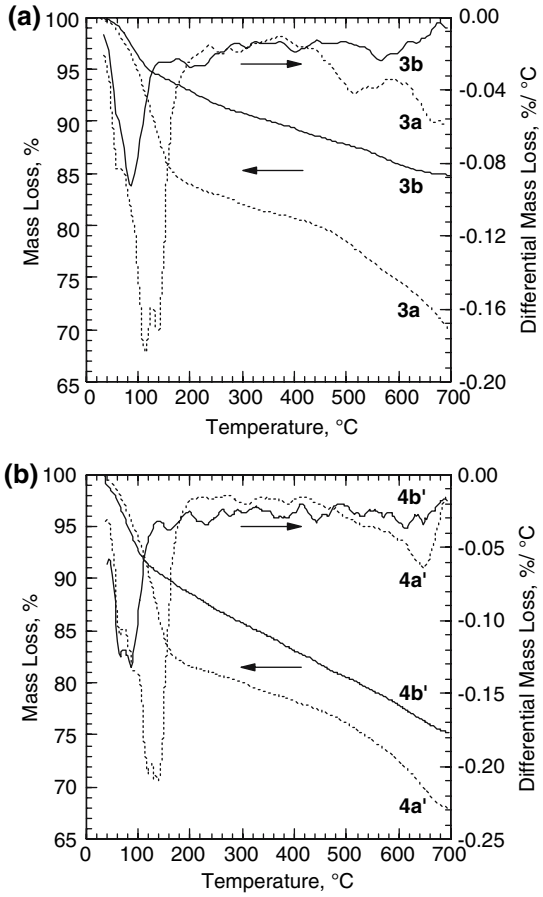

Fig. 5 The thermogravimetric analysis of catalysts **3a**, dashed curves, and **3b**, solid curves, (**a**) and **4a′**, dashed curves, and **4b′**, solid curves, (**b**)

Transmission electron microscopy

The composites obtained by carbon vapor deposition on the four catalysts have been characterized by transmission electron microscopy with a Philips Tecnaï 10 microscope. Typical images are shown in Fig. 6 where the large black areas correspond to platelets of the clay catalyst. The distribution of the number of nanotube walls and the internal and external diameters of the tubes have been determined from the micrographs by measuring at least 100 nanotubes per sample by using the METRIC7.1 program.

For nanotubes prepared with **3a** and **3b**, the catalysts prepared by mechanical agitation, the 200 nm transmission

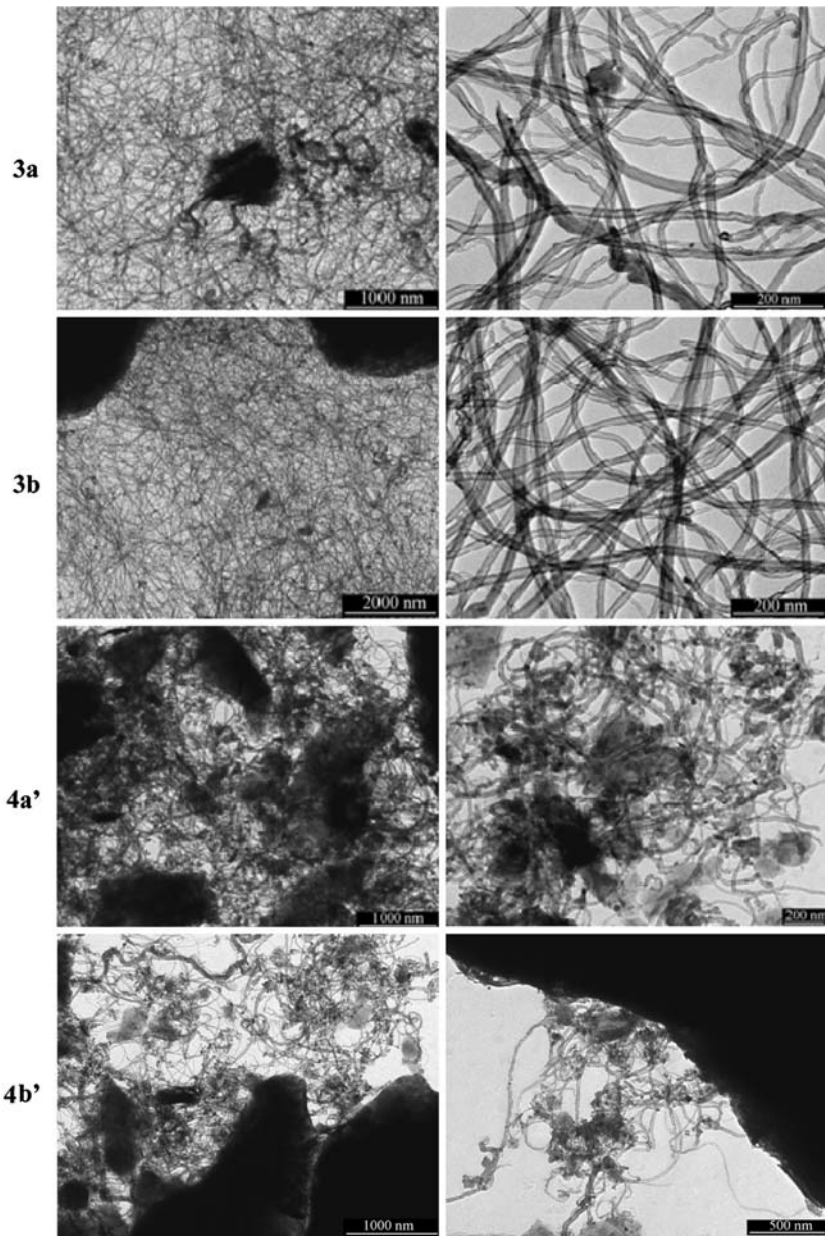

Fig. 6 Transmission electron micrographs of catalysts **3a**, **3b**, **4a'**, and **4b′**, from top to bottom

electron micrographs confirm the presence of multiwall carbon nanotubes; the number of walls and the internal and external diameters of the nanotubes are given in Table 4 and their distribution is shown in Fig. 7. In the case of catalyst **3a**, a higher yield of multiwall carbon nanotubes was obtained but carbon fibers were also obtained, as is indicated by the darker fibers seen at both 1,000 nm and 200 nm magnification. In contrast, the carbon nanotubes prepared with catalyst **3b** are more uniform and have fewer defects than those of **3a** as is most easily seen at 200 nm magnification in Fig. 6.

Table 4 Characteristics of the carbon nanotubes

Catalyst	Number of walls	Internal diameter, nm	External diameter, nm	Wall thickness, nm
3a	16 (5)	10.9 (3)	22.1 (4)	0.75
3b	15 (4)	9.9 (3)	20.1 (4)	0.68
4a′	18 (5)	9.1 (2)	19.7 (3)	0.59
4b′	16 (4)	8.6 (2)	20.8 (4)	0.76

For catalysts **4a′** and **4b′**, prepared by sonication, the transmission electron micrographs show a poor graphitization of the multiwall carbon nanotubes as is indicated by the dark areas along the tubes and the presence of amorphous carbon, i.e., carbon that shows only short range organization, that appears as the diffuse grey areas at 200 nm and 500 nm magnification. The number of walls for the carbon

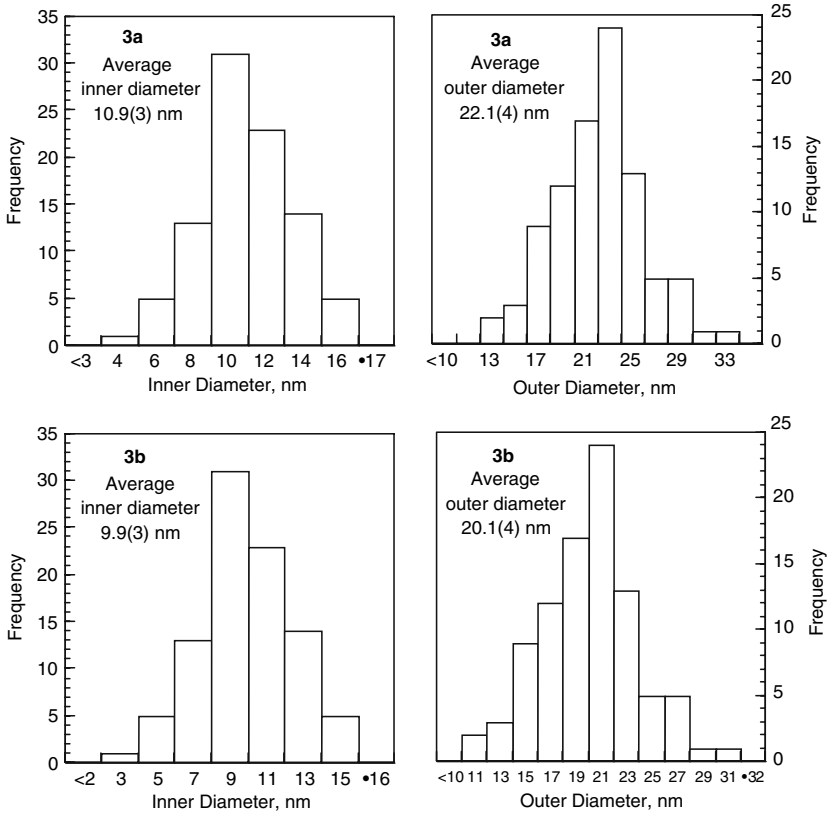

Fig. 7 The distributions of the inner and outer diameters for catalysts **3a**, top, and **3b**, bottom

nanotubes grown on catalysts **4a′** and **4b′** is given in Table 4 and their distribution is shown in Fig. 8. These less satisfactory nanotubes resulting from the use of the **4a′** and **4b′** catalysts may be related to the size of the cobalt and iron particles present in the catalysts. Indeed, previous studies [18] have shown that the formation of carbon nanotubes by catalytic decomposition of hydrocarbons requires metal clusters that are both uniform in size and distribution and sufficiently far apart from each other to both prevent segregation of the particles on the supporting surface, a segregation that can lead to a deactivation of the catalyst.

The numbers of walls and the external diameters of the carbon nanotubes given in Table 4 are the same within their error limits for the four catalysts and, hence, do not depend on the preparation method of the catalysts. Only the internal diameters shows a decreasing trend from catalyst **3a** to **4b′**, a trend that could be the result of a decrease in size of the anchoring particles. Further, the internal diameters of the nanotubes grown on catalysts **3b** and **4b′**, catalysts that have been centrifuged, are smaller than those of the nanotubes grown on catalysts **3a** and **4a′**, catalysts that have not been centrifuged. This behavior indicates that both sonication and centrifugation result in smaller anchoring particles for the growth of carbon nanotubes. These observations can be understood in terms of a proposed carbon nanotube growth process [19] on supported metal catalysts, a process that is schematically represented in Fig. 9. In this process, the size of the transition metal particle determines the size of the carbon nanotubes. The washing of the catalysts favors small particles, through the elimination of metal salts and the prevention of agglomeration of the particles, and hence leads to narrower carbon nanotubes.

Hence, it seems that a combination of transition-metal content, size, and the distribution of the anchoring transition-metal particles influences the amount and quality of the nanotubes. The catalyst that gives the best quality carbon nanotubes is **3b**, a catalyst that has been prepared by mechanical agitation and subsequent washing and centrifugation.

Mössbauer spectral results

The Mössbauer spectra have been measured at 85 K and 295 K on a constant-acceleration spectrometer which utilized a rhodium matrix cobalt-57 source and was calibrated at room temperature with α-iron foil. The Mössbauer spectral absorber of the Na Cloisite® was a 200 mg pressed pellet. The Mössbauer spectral absorbers of the catalysts, of the calcined catalysts, and of the carbon-nanotube clay composites contained ca. 25 mg/cm^2 of powdered sample mixed with boron nitride. The Mössbauer spectral

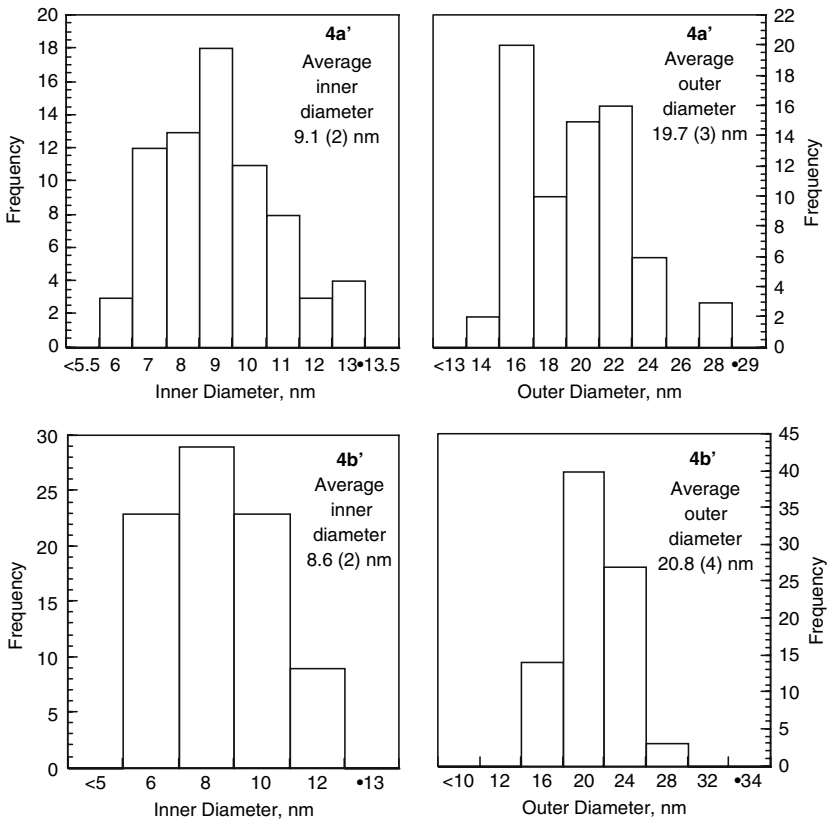

Fig. 8 The distributions of the inner and outer diameters for catalysts **4a′**, top, and **4b′**, bottom

absorbers of the separated carbon nanotubes were obtained on pressed pellets of 200–500 mg of the four samples. The spectra have been fit as discussed below and the estimated relative errors are at most ±0.1 T for the hyperfine fields, ±0.005 mm/s for the isomer shifts, ±0.01 mm/s for the quadrupole splittings and quadrupole shifts, and ±0.2% for the relative areas. The absolute errors are probably twice as large.

The Mössbauer spectra of Na Cloisite® shown in Fig. 10 will be discussed first followed in order by those of the catalysts, the calcined catalysts, the composite materials, and the resulting nanotubes. The spectra are shown in this order in Figs. 11–14.

Na cloisite® Mössbauer spectra

The 85 K and 295 K iron-57 Mössbauer spectra of the Na Cloisite® starting material are shown in Fig. 10. The 85 K Mössbauer spectrum of the Na Cloisite® obtained at large velocity range of ±12 mm/s (not shown) indicates that ca. 12% of the iron(III) ions are magnetically ordered with a maximum hyperfine field of 53.8 T, a field that is characteristic [20] of α-Fe_2O_3. The large line width of ca. 1.6 mm/s of the two sextets used to fit this magnetic contribution indicates that this iron oxide is present in small particles that are likely to be paramagnetic at 295 K and are hidden under the main contributions to the spectrum.

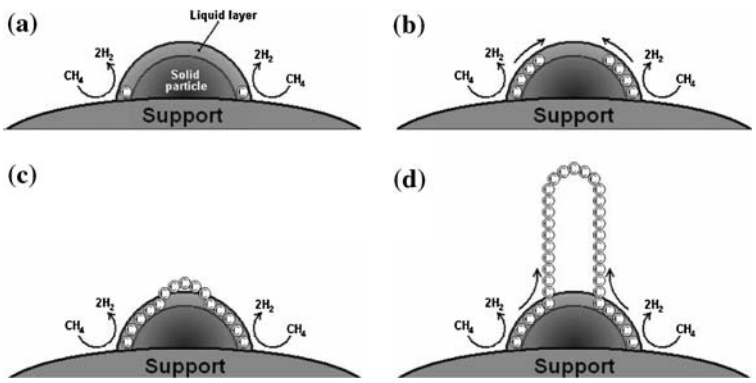

Fig. 9 A schematic diagram of the proposed growth of carbon nanotubes by carbon chemical vapor deposition. (**a**) Adsorption and decomposition of the hydrocarbon. (**b**) Carbon diffusion in the liquid surface layer of the particle. (**c**) Supersaturation of the surface and formation of the cap. (**d**) Growth of the carbon nanotube

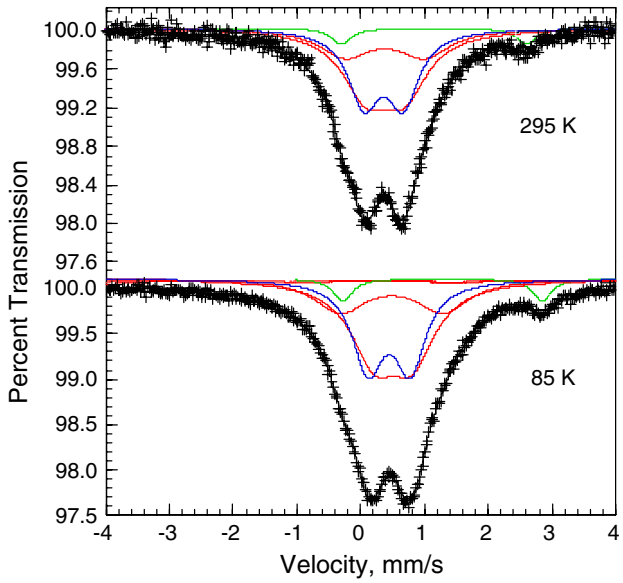

Fig. 10 The Mössbauer spectra of Na Cloisite® obtained at 85 K and 295 K

Superparamagnetic α-Fe_2O_3 typically exhibits [21] an isomer shift of 0.34 mm/s and a quadrupole splitting of 0.75 mm/s at 295 K. These superparamagnetic particles of α-Fe_2O_3 are very similar to those observed [22] previously in a clay separated from a Greek soil.

Different attempts to fit the 85 K and 295 K spectra shown in Fig. 10 with three doublets, as was previously proposed for the spectra of dioctahedral smectites [23] and of montmorillonite [10, 24] were completely unsuccessful. Satisfactory fits of the spectra at both 85 K and 295 K required four symmetric doublets, with the spectral parameters given in Table 5. Doublets one and two are assigned [25, 26] to iron(III) in the *M*1 and *M*2 octahedral sites and their relative areas have been constrained in the ratio of 1:2. The hyperfine parameters of the *M*1 and *M*2 doublets agree with those observed [10] in the Zenith N, reported fits in which the area ratio constrain was not used. There are two possible assignments for doublet three; it may be assigned to iron(III) in the tetrahedral site because of its smaller isomer shift, or alternatively, it could either be assigned to iron(III) in an impurity phase present in the clay or to a small amount of non-clay impurity that is not detected by X-ray diffraction. In view of its relative area of 33%, the first assignment of doublet three is preferred and is used throughout this paper. Doublet four, with a relative area of ca. 5%, is assigned [24] to iron(II) ions in the octahedral site. The above assignment of the four doublets is not instrumental in the subsequent analysis of the Mössbauer spectra of the catalysts, composites and nanotubes. However, it is important to note that the Mössbauer spectra indicate only the different types of

Fig. 11 The Mössbauer spectra of **3a** obtained at 295 K, **a**, and 85 K, **b**

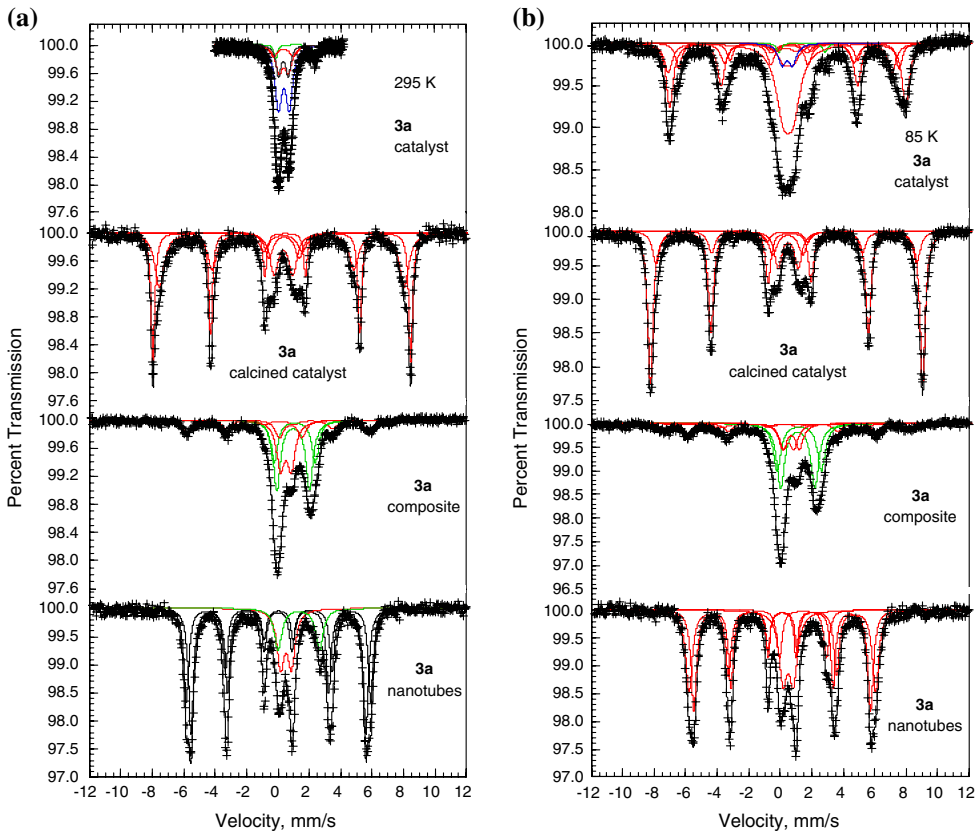

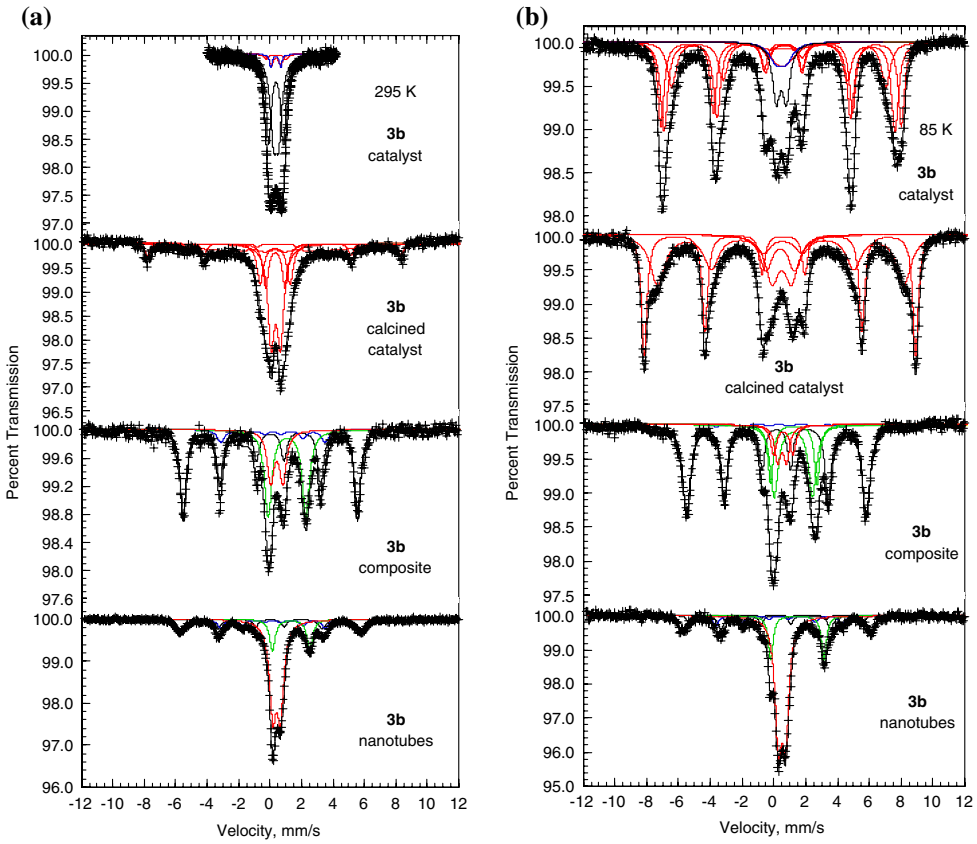

Fig. 12 The Mössbauer spectra of **3b** obtained at 295 K, **a**, and 85 K, **b**

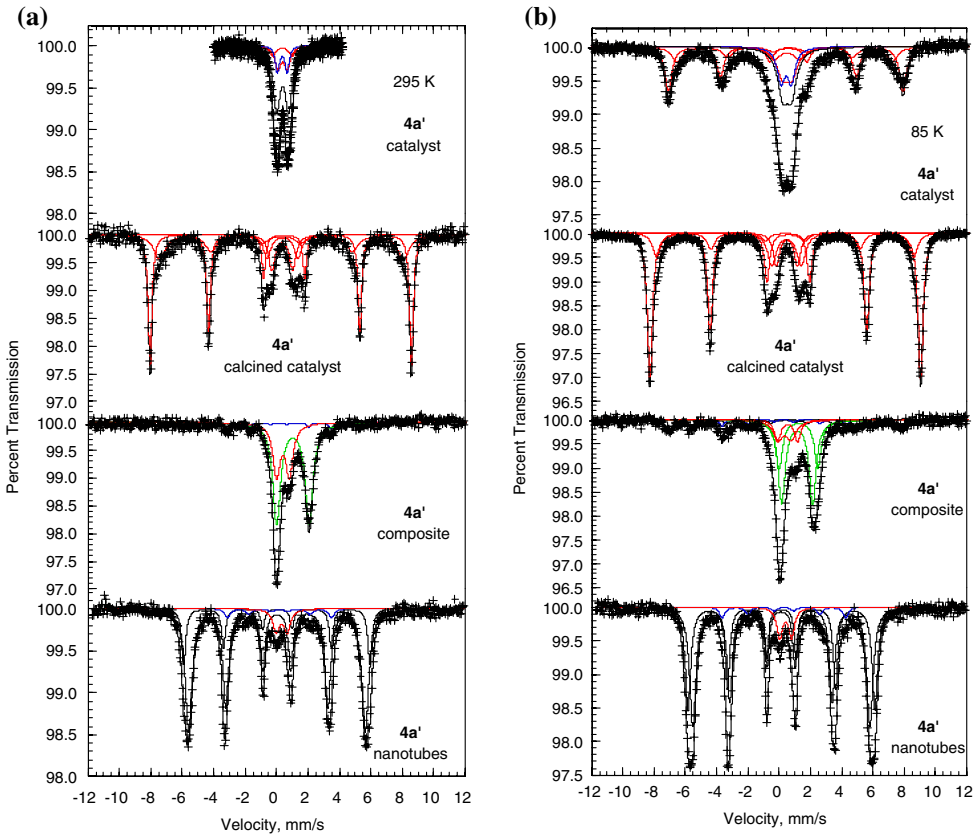

Fig. 13 The Mössbauer spectra of **4a'** obtained at 295 K, **a**, and 85 K, **b**

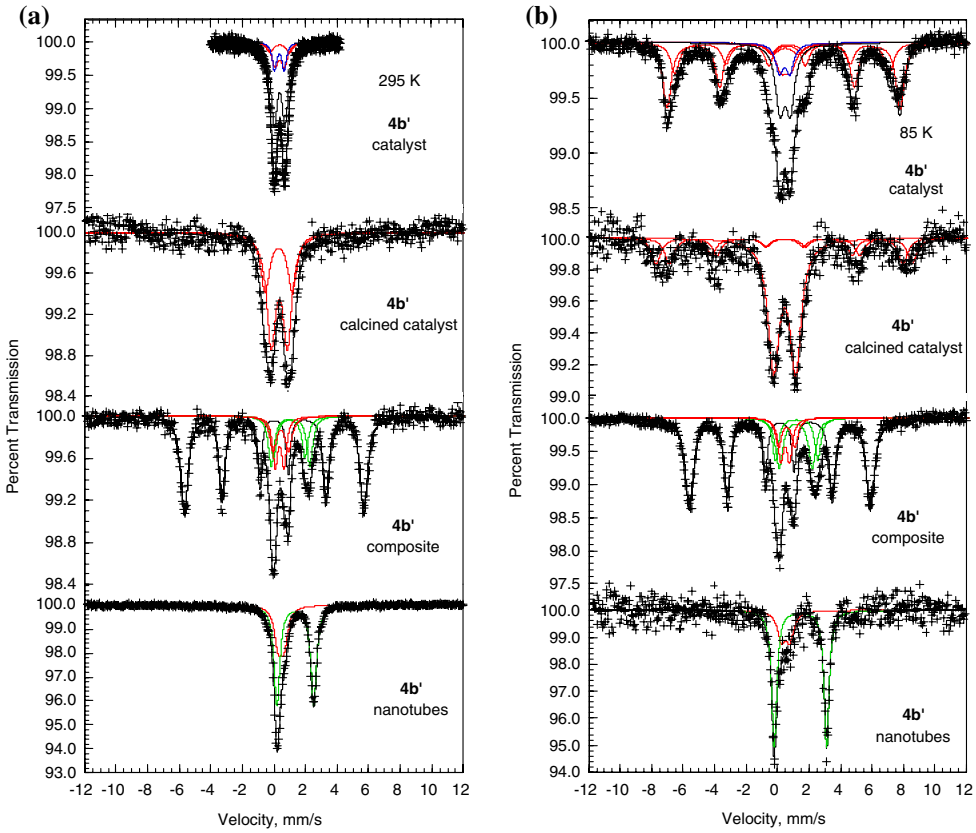

Fig. 14 The Mössbauer spectra of **4b'** obtained at 295 K, **a**, and 85 K, **b**

iron-containing species present, species that represent only ca. 4% of the starting Na Cloisite® material.

Mössbauer spectra of the catalysts

The Mössbauer spectra of the catalysts, **3a**, **3b**, **4a′** and **4b′**, obtained at 85 K and 295 K are shown at the top of Figs. 11–14, respectively. The hyperfine parameters for sample **3b** are given in Table 5 and those for samples **3a**, **4a′** and **4b′** are given in Tables A1–A3 in the appendix. At 295 K the spectra of the four catalysts have been fitted with three iron(III) doublets and one additional iron(II) doublet for catalyst **3a**. The hyperfine parameters and relative areas of the three iron(III) doublets, numbers one to three in Table 5, have been constrained to be identical to those observed in the Na Cloisite®; the line widths have been fitted and are significantly narrower than those observed in the Na Cloisite®. In catalyst **3a**, the hyperfine parameters of the iron(II) doublet are significantly different from those observed in the Na Cloisite® and its relative area is larger than that observed in the Na Cloisite®. This iron(II) doublet may well be related to the presence of iron(II) chlorides—as well as cobalt(III) chlorides—observed in the X-ray diffraction pattern of catalyst **3a**. A satisfactory fit of the spectra of catalysts **3a**, **4a′** and **4b′**, requires one additional iron(III) doublet, whereas the fit of catalyst **3b** requires two additional iron(III) doublets. The insertion of cobalt(II) and iron(III) in the clay has clearly removed the iron(II) ions naturally present in the clay for all samples except **3a**. As expected, the 295 K spectra of catalysts, **3b**, **4a′** and **4b′**, show a decrease in the relative areas of doublets one to three as compared to the Na Cloisite®. The hyperfine parameters of doublet five in the spectra of catalysts,**3a**, **4a′** and **4b′** and of doublets four and five in **3b** are comparable to those [21] of superparamagnetic α-Fe_2O_3, i.e., small particles of α-Fe_2O_3. The relative area of these doublets indicates that 53.6%, 90.6%, 58.2% and 59.0% of the iron is superparamagnetic at 295 K in catalysts **3a**, **3b**, **4a′** and **4b′**, respectively. These particles are probably too small to be observed in the X-ray diffraction patterns.

At 85 K, the Mössbauer spectra of the four catalysts, **3a**, **3b**, **4a′** and **4b′**, exhibit magnetically ordered components, components that have been fit with two or three sextets, with a total relative area of 55.6%, 75.7%, 45.7% and 57.9%, respectively. The paramagnetic components in the 85 K spectra have been fitted with four, for **3a**, or three, for **3b**, **4a′** and **4b′**, doublets with hyperfine parameters and relative areas similar or identical to those observed in the Na Cloisite®. An additional fifth doublet, with hyperfine parameters similar to those observed at 295 K was required to obtain a satisfactory fit. The total relative areas of the sextets and doublet five are 83.9%, 85.1%, 66.6% and 77.8%, in

Table 5 Mössbauer spectral parameters for Na cloisite® and sample **3b**

T, K	Parameter	Na cloisite®	Assign.	Catalyst	Assign.	Calcined catalyst	Assign.	Composite	Assign.	Carbon nanotubes	Assign.
295	δ_1,[a] mm/s	0.373	Fe^{3+} *M*1	0.373	Fe^{3+} *M*1	0.319	Fe^{3+}	0.419	Fe^{3+}	0.412	Fe^{3+}
	$\Delta E_{Q,1}$, mm/s	1.24		1.24		1.89		0.77		0.493	
	Γ_1, mm/s	0.972		0.312		0.486		0.587		0.497	
	A_1, %	20.7		2.1		15.6		18.0		53.5	
	δ_2,[a] mm/s	0.380	Fe^{3+} *M*2	0.380	Fe^{3+} *M*2	0.334	Fe^{3+}	1.067	Fe^{2+}	1.344	Fe^{2+}
	$\Delta E_{Q,2}$, mm/s	0.60		0.60		1.23		2.39		2.36	
	Γ_2, mm/s	0.891		0.287		0.426		0.566		0.522	
	A_2, %	41.4		4.1		14.8		30.9		20.5	
	δ_3,[a] mm/s	0.358	Fe^{3+} T_d	0.358	Fe^{3+} T_d	0.364	Fe^{3+}	–			
	$\Delta E_{Q,3}$, mm/s	0.62		0.62		0.59		–			
	Γ_3, mm/s	0.592		0.191		0.507		–			
	A_3, %	33.2		3.3		38.2		–			
	δ_4,[a] mm/s	1.143	Fe^{2+}	0.381	Fe^{3+} SP	0.318	Fe^{3+} ox.	0.017	FeCo	0.055	FeCo[c]
	$\Delta E_{Q,4}$, mm/s	2.90		0.33		–		–		–	
	H_4, T	–		–		24.9		34.3		35.3	
	Γ_4, mm/s	0.366		0.502		1.056		0.453		0.479	
	A_4, %	4.6		45.3		23.4		51.1		26.1	
	δ_5,[a] mm/s	–	–	0.37	Fe^{3+} SP	0.366	Fe^{3+} ox.	0.18	Fe_3C	0.18	Fe_3C
	$\Delta E_{Q,5}$, mm/s	–	–	0.94		–		–		–	
	H_5, T	–	–	–		50.0		20.5		20.5	
	Γ_5, mm/s	–	–	0.410		0.361		0.554		0.495	
	A_5, %	–	–	45.3		8.2		8.2		10.6	
85[b]	δ_1,[a] mm/s	0.485	Fe^{3+} *M*1	0.485	Fe^{3+} *M*1	0.319	Fe^{3+}	0.513	$Fe^{3+,\ c}$	0.508	Fe^{3+}
	$\Delta E_{Q,1}$, mm/s	1.61		1.61		1.85		0.86		0.442	
	Γ_1, mm/s	0.972		1.617		0.956		0.470		0.513	
	A_1, %	15.3		3.2		11.0		14.7		56.3	
	δ_2,[a] mm/s	0.509	Fe^{3+} *M*2	0.510	Fe^{3+} *M*2	0.481	Fe^{3+}	1.211	$Fe^{2+,\ c}$	1.470	Fe^{2+}
	$\Delta E_{Q,2}$, mm/s	0.60		0.60		1.22		2.58		3.31	
	Γ_2, mm/s	0.891		1.483		1.012		0.521		0.561	
	A_2, %	30.6		6.4		16.0		32.4		21.7	
	δ_3,[a] mm/s	0.443	Fe^{3+} T_d	0.443	Fe^{3+} T_d	–	–	–	–	–	
	$\Delta E_{Q,3}$, mm/s	0.66		0.66		–	–	–	–	–	
	Γ_3, mm/s	0.592		0.985		–	–	–	–	–	
	A_3, %	24.5		5.2		–	–	–	–	–	
	δ_4,[a] mm/s	1.282	Fe^{2+}	–		0.464	Fe^{3+} ox.	0.132	FeCo	0.103	FeCo[c]
	$\Delta E_{Q,4}$, mm/s	3.13		–		–		–		–	
	H_4,T	–		–		47.9		35.0		36.7	
	Γ_4, mm/s	0.366		–		1.105		0.351		0.348	
	A_4, %	3.9		–		37.0		52.0		22.0	
	δ_5,[a] mm/s	–		0.462	Fe^{3+} SP	0.486	Fe^{3+} ox.	0.298	Fe_3C	0.298	Fe_3C
	$\Delta E_{Q,5}$, mm/s	–		0.63		–		–		–	
	H_5,T	–		–		52.8		24.5		24.5	
	Γ_5, mm/s	–		0.569		0.413		0.501		0.409	
	A_5, %	–		9.4		36.0		1.0		8.22	

[a] Relative to room temperature α-iron foil

[b] If the relative areas do not sum to 100%, there are unreported magnetic sextet contributions to the spectrum, see text

[c] The average values of two components

rough agreement with the relative area of doublet number five at 295 K. It is clear that the overlap of the five doublets in the 295 K spectra does not permit a very accurate determination of the relative areas of these doublets.

The observed sextets are assigned to superparamagnetic particles of α-Fe_2O_3 or other iron oxides or oxyhydroxides with slow magnetic relaxation on the Mössbauer-effect timescale. Their hyperfine fields range between 41.8 T and 46.8 T and are smaller than the expected field of 53 T for ferromagnetic α-Fe_2O_3 at 85 K. They are also smaller than the fields of 49 and 52.1 T observed [27] at 80 K in $CoFe_2O_4$. However, the observed magnetic contribution in Fig. 11 is quite similar to that observed [28] for nanowires of $CoFe_2O_4$ grown inside carbon nanotubes. Finally, 80 Å particles of $CoFe_2O_4$ give a Mössbauer spectrum [29] at 80 K that is very similar to those observed herein. Hence, it is tempting to assign the magnetic contribution to small particles of $CoFe_2O_4$, a spinel that is present in the X-ray diffraction pattern of the calcined catalysts. However, small particles of α-Fe_2O_3 or another iron oxide or oxyhydroxide, such as β-FeOOH or akaganeite, may give the same type of spectra. The 85 K spectra of the catalysts are very similar to those previously reported [30] for magnetically modified pillared clays, in which the magnetic sextet was assigned to γ-Fe_2O_3.

The spectra for catalyst **3a** are similar to the spectrum [31] observed for a montmorillonite loaded with $Fe(NO_3)_3$, a low-resolution spectrum that has been analyzed with two iron(III) and one iron(II) doublets.

In conclusion, both the 295 K and 85 K Mössbauer spectra of catalysts **3a**, **3b**, **4a′** and **4b′**, indicate that a substantial fraction, ca. 75%, of the iron ions are present as small particles of iron oxides. It is difficult to establish the exact nature of these oxides, because the hyperfine fields of different iron oxides in small particles are very similar. The size of the small particles may be estimated [20] to be ca. 10 nm from the observed blocking temperature of between 85 K and 295 K. It is interesting to note that catalyst **3b**, the catalyst that produces the best carbon nanotubes, also yields the largest amount of small iron oxide particles. From the Mössbauer spectra, it cannot be established whether these small particles are formed on the surface of the clay particles or are intercalated between the clay layers and form the so-called pillars. However, the similarity between the estimated size of 10 nm and the inner diameter of the carbon nanotubes supports the belief that the nanotubes grow on these particles.

Mössbauer spectra of the calcined catalysts

The Mössbauer spectra of calcined catalysts **3a**, **3b**, **4a′** and **4b′**, obtained at 85 K and 295 K are shown in Figs. 11–14, respectively. The spectra of **3a** and **4a′** are similar and show little change with temperature, whereas the spectra of **3b** and **4b′** show substantial and different changes with temperature. All the spectra have been fit with two sextets and two or three doublets as required; the resulting Mössbauer spectral hyperfine parameters are given in Tables 5 and A1 to A3. At both 85 and 295 K as expected, all the components have isomer shifts that are characteristic of iron(III) after calcination at 700 °C.

At 295 K the three calcined catalysts **3a**, **3b** and **4a′** show both paramagnetic and magnetic components, whereas **4b′** shows a major and significantly different paramagnetic component as well as a minor broad magnetic component. At 85 K, all four samples show both paramagnetic and magnetic components, with a substantial increase in the relative area of the magnetic components. This behavior indicates that the samples contain a large fraction of small particles of iron(III) that are superparamagnetic at room temperature and are blocked on the Mössbauer time scale at 85 K. Sample **4b′** contains the smallest amount of magnetic components, whereas samples **3a** and **4a′** contain the largest amount. It may be concluded that the particles are smaller in **4b′** than in **3a** and **4a′**, in agreement with the proposal that washing favors the presence of small transition-metal particles. The quadrupole splittings of doublets one and two, observed at both 85 K and 295 K, are large but may be assigned [21] to iron(III) ions in strongly distorted octahedral sites. Doublet three in **3b** is assigned to superparamagnetic particles of α-Fe_2O_3. The quadrupole splittings of doublets one and two at 295 K in **4b′** are different from those observed in the other three samples and may be related to iron(III) ions present in a different oxide or hydroxide phase, such as the CoOOH detected in the X-ray diffraction pattern of this sample.

The presence of $CoFe_2O_4$ has been detected by X-ray diffraction in **3a** and **4a′**. The hyperfine fields and isomer shifts observed in the 295 K and 85 K spectra of the calcined catalysts **3a** and **4a′** are compatible with those [27] of $CoFe_2O_4$. The hyperfine fields observed in the 85 K spectra of the calcined catalysts **3b** and **4b′** are smaller and may indicate the presence of a different iron(III) oxide.

Mössbauer spectra of the composites

The Mössbauer spectra of the carbon-nanotube catalyst composites, **3a**, **3b**, **4a′** and **4b′**, obtained at 85 K and 295 K are shown in Figs. 11–14, respectively. The spectra show virtually no change with temperature. However, the spectra of **3b** and **4b′** are similar and similar to the ZNa-C_2H_2 spectrum [10] but different from those of **3a** and **4a′**, spectra that are also similar. The difference resides in the presence of ca. 10% of a broad sextet characteristic of an iron oxide or oxyhydroxide in the spectra of **3a** and **4a′**,

oxides that were already present in catalysts **3a** and **4a′**. Hence, the washing of the catalyst eliminates this component in the carbon-nanotube catalyst composites. The nonmagnetic components have been analyzed with up to four doublets, whereas the magnetic components have been analyzed with up to three sextets. The resulting Mössbauer spectral parameters are given in Tables 5 and A1–A3. Two doublets with the average hyperfine parameters reported as one in Table 5 are assigned to iron(III) and two doublets with average hyperfine parameters reported as two in Table 5 are assigned to iron(II). These doublets are very similar to both those observed [23] for montmorillonite reduced with hydrazine and for ZFe-C_2H_2 [10]. Doublet five in Tables A1 and A3 may tentatively be assigned [32] to Fe_2SiO_4. The isomer shift and hyperfine field of sextet four are characteristic [33, 34] of metallic iron in an FeCo alloy. It is obvious both from Figs. 11–14 and from Tables 5 and A1 to A3 that samples **3a** and **4a′** contain only approximately 12% and 7% of the FeCo alloy, whereas samples **3b** and **4b′** contain approximately 50% of this alloy. Hence, the Mössbauer spectra indicate that a reduction of the iron oxidation state has taken place during carbon deposition, a reduction that is in agreement with the reducing properties of ethylene. Further, a larger fraction of the transition-metal anchors are present in the form of an FeCo alloy in the composites that have been prepared on the washed catalysts **3b** and **4b′**. Indeed, in the case of catalyst **3b**, these numerous FeCo anchors lead to an extensive formation of carbon nanotubes.

In the 295 K spectrum of the **4a′** composite, see Fig. 13a, there is a clear weak sextet five in Table A2. The small absorption present at ca. –2 mm/s in the 295 K spectrum of the **3b** composite, see Fig. 12a, is indicative of the presence of the same sextet, whose hyperfine parameters are characteristic of cementite, Fe_3C. It is interesting to note that in the spectra of the **3a** and **4b′** composites, this sextet is absent but the Fe_2SiO_4 doublet is present. This observation supports the growing process [32] of carbon nanotubes, a process in which Fe(III) is first partially reduced to Fe(II) before it is fully reduced to Fe(0) in the FeCo alloy and cementite, Fe_3C.

The hyperfine fields observed at 295 K for the FeCo sextets in the **3a**, **3b** and **4b′** spectra are plotted in Fig. 15 as a function of the number of *d* electrons per metal atom in the FeCo alloy, together with the hyperfine fields measured in bulk [33] and in various small particles [34–36] of FeCo alloys. The data between 6.0 *d* and 6.6 *d* electrons per atom have been fit with a third-order polynomial. From the observed hyperfine fields, 6.39, 6.55, and 6.48 *d*-electrons are obtained for **3a**, **3b** and **4b′**, respectively. Hence, the composition of the all the alloys are between $Fe_{39}Co_{61}$ and $Fe_{55}Co_{45}$, in good agreement with the 50:50 composition of the transition metal salt solutions used for the cationic exchange.

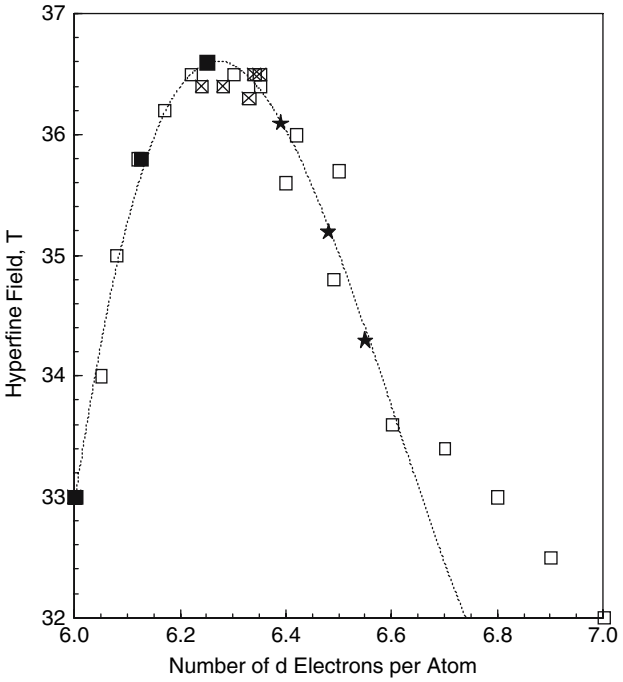

Fig. 15 The average hyperfine field as a function of the number of 3*d* electrons in the FeCo alloys. The open squares represent values measured[32] for bulk FeCo alloys, the crossed squares values measured[33] for small FeCo alloy particles, and the solid squares represent values measured[34,35] for nanopowders of FeCo alloys, the stars represent the values measured herein

Because at this point in this study, there is only an indication of the presence or influence of carbon upon the iron-57 Mössbauer spectra of the **3b** and **4a′** composites, the four composites have been washed with concentrated hydrofluoric acid, filtered, and then washed with concentrated hydrochloric acid, in an attempt to recover the nanotubes with the iron atoms or ions that are attached or encapsulated by the nanotubes.

Mössbauer spectra of the carbon nanotubes

The Mössbauer spectra of the nanotubes are shown at the bottom of Figs. 11–14. Except for **4b′**, that exhibits only doublets, all other samples exhibit sextets and doublets. The spectra have been analyzed with two doublets and up to three sextets; the resulting hyperfine parameters are given in Tables 5 and A1 to A3. The parameters of sextet four are characteristic of an FeCo alloy and those of sextet five of Fe_3C. Doublets one and two are assigned to iron(III) and iron(II) ions, respectively. The relative area of the FeCo sextets in **3b** is much smaller than in **3a** and **4a′**, whereas the relative area of Fe_3C, ca. 9%, is larger than in **4a**, ca. 4%. Finally, the 295 K and 85 K spectra of the nanotubes **4b′** exhibit only the presence of two doublets assigned to iron(III) and iron(II) ions, most likely present as fluorides. The absence of the sextet characteristic of an

FeCo alloy in the **4b′** nanotubes seems to indicate that this alloy was not protected by the carbon nanotubes and consequently was transformed in iron and cobalt fluorides by the hydrofluoric acid treatment. This interpretation is confirmed by the transmission electron microscopic analysis which indicated that the carbon deposit on **4b′** consisted mostly of fibers and amorphous carbon.

Discussion and conclusions

Extensive information has been gained through the Mössbauer spectral study of Na Cloisite®, the resulting catalysts, calcined catalysts, carbon-nanotube catalyst composites, and the carbon nanotubes. It is worthwhile discussing this information in view of that gained through other techniques and previously published results on similar materials with the goal of identifying the anchors and the growth process of the carbon nanotubes.

The Mössbauer spectra of the catalysts obtained after ionic exchange on montmorillonite indicate that 50–75% of the iron is present as an iron oxide or oxyhydroxide. The formation of this oxide or oxyhydroxide is not surprising in view of the preparative method used herein. Indeed, the iron is introduced as iron(III) chloride and mixed in aqueous solution with the clay at 80°C, see experimental section. The decomposition of the iron(III) chloride proceeds according to the reaction $2FeCl_3 + 3\ H_2O \leftrightarrow Fe_2O_3 + 6\ HCl$.

Both transmission electron micrographs and Mössbauer spectra indicate that the washed **b** catalysts have a larger number of smaller FeCo anchoring particles for the growth of carbon nanotubes and, as a result, the carbon nanotubes grown on these catalysts have smaller inner diameters. If the FeCo alloy formed at the surface of the clay is assumed to be an anchor for the carbon nanotubes, then the relative area, A4, of the FeCo alloy Mössbauer spectral sextet in the composites may be related to the efficiency of the catalyst to grow nanotubes; in this case **3b** and **4b′** would be the best catalysts. For catalyst **3b**, this is the case in terms of the quality of the resulting carbon nanotubes that show fewer defects and no amorphous carbon; in catalyst **4b′**, this is not the case. The different efficiencies of **3b** and **4b′** may be related to their different thermal behavior, a behavior that leads to differences in the resulting carbon nanotubes. Further, the presence of Fe_3C in the spectra of the **3b** and **4a′** composites and nanotubes, as well as its absence in those of **4b′**, indicate the existence of chemical bonding in the former samples and its absence in the latter. The amount of cementite observed in **3b** and **4a′** composites and nanotubes is certainly smaller than was observed [10, 32] earlier. There is no doubt that the addition of cobalt in the synthesis of the samples studied herein is responsible for this reduction. It is indeed well known [37, 38] that the addition of cobalt in steels hinders the formation of cementite.

In contrast with previous Mössbauer spectral studies [10, 39, 40] of iron encapsulated in carbon nanotubes, the presence of γ-iron, which is characterized by a single line at ca. 0 mm/s, has *not* been detected in the samples studied herein. The presence of cobalt and the stability of the bcc FeCo phase appear to suppress the formation of γ-iron.

In conclusion, a large number of carbon nanotubes have been grown on montmorillonite clay intercalated with iron and cobalt ions. The best quality deposit of carbon nanotubes was obtained on a sodium containing clay exchanged with three times its cation exchange capacity through mechanical agitation and subsequent centrifugation. The Mössbauer spectra indicate that these carbon nanotubes grow on small iron oxide particles that are subsequently reduced to an FeCo alloy through the carbon vapor deposition process.

Acknowledgments The authors thank Ms. Nathalie Fagel, Dr. Leïla Rebbouh, and Prof. André Rulmont for their help during the course of this work and the referee for helpful comments. The authors acknowledge the financial support of the Ministère de la Région Wallone for grant number RW/115012 and the BINANOCO project, and of the Fonds National de la Recherche Scientifique, Belgium for grant 1.5.064.05.

Appendix

Table A1 Mössbauer spectral parameters for cloisite and sample **3a**

T, K	Parameter	Na cloisite®	Assign.	Catalyst	Assign.	Calcined catalyst	Assign.	Composite	Assign.	CNT	Assign.
295	δ_1,[a] mm/s	0.373	Fe^{3+} *M*1	0.373	Fe^{3+} *M*1	0.404	Fe^{3+}	0.519	Fe^{3+}	0.505	Fe^{3+}
	$\Delta E_{Q,1}$, mm/s	1.24		1.24		1.93		0.68		0.689	
	Γ_1, mm/s	0.972		0.615		0.625		0.614		0.562	
	A_1, %	20.7		10.4		8.1		23.6		14.1	
	δ_2,[a] mm/s	0.380	Fe^{3+} *M*2	0.380	Fe^{3+} *M*2	0.366	Fe^{3+}	0.986	Fe^{2+}	1.321	Fe^{2+}
	$\Delta E_{Q,2}$, mm/s	0.60		0.60		1.19		2.08		2.63	
	Γ_2, mm/s	0.891		0.565		0.714		0.546		0.575	

Table A1 continued

T, K	Parameter	Na cloisite®	Assign.	Catalyst	Assign.	Calcined catalyst	Assign.	Composite	Assign.	CNT	Assign.
	A_2, %	41.4		20.8		13.1		31.8		10.9	
	δ_3,[a] mm/s	0.358	Fe^{3+} T_d	0.358	Fe^{3+} T_d	–		0.818	Fe^{3+}	–	
	$\Delta E_{Q,3}$, mm/s	0.62		0.62		–		1.43		–	
	Γ_3, mm/s	0.592		0.375		–		0.623		–	
	A_3, %	33.2		16.7		–		9.2		–	
	δ_4,[a] mm/s	1.143	Fe^{2+}	1.130	Fe^{2+}	0.297	Fe^{3+} ox.	0.088	FeCo	0.015	FeCo
	$\Delta E_{Q,4}$, mm/s	2.90		2.51		–		–		–	
	H_4,T	–		–		48.3		36.1		34.5	
	Γ_4, mm/s	0.366		0.260		0.714		0.728		0.379	
	A_4, %	4.6		5.7		39.5		16.0		43.0	
	δ_5,[a] mm/s	–		0.391	Fe^{3+} SP	0.368	Fe^{3+} ox.	1.078	Fe^{2+}	0.035	FeCo
	$\Delta E_{Q,5}$, mm/s	–		0.69		–		2.62		–	
	H_5,T	–		–		50.8		–		36.4	
	Γ_5, mm/s	–		0.525		0.282		0.535		0.379	
	A_5, %	–		46.4		39.2		19.4		32.1	
85[b]	δ_1,[a] mm/s	0.485	Fe^{3+} *M*1	0.349	Fe^{3+} *M*1	0.478	Fe^{3+}	0.612	$Fe^{3+,\ c}$	0.506	Fe^{3+}
	$\Delta E_{Q,1}$, mm/s	1.61		1.34		1.90		0.863		0.648	
	Γ_1, mm/s	0.972		0.972		0.640		0.599		0.619	
	A_1, %	15.3		3.2		7.8		23.0		18.4	
	δ_2,[a] mm/s	0.509	Fe^{3+} *M*2	0.516	Fe^{3+} *M*2	0.503	Fe^{3+}	1.153	$Fe^{2+,\ c}$	1.447	Fe^{2+}
	$\Delta E_{Q,2}$, mm/s	0.60		0.61		1.27		2.45		2.99	
	Γ_2, mm/s	0.891		0.891		0.559		0.600		0.402	
	A_2, %	30.6		6.4		10.6		53.6		8.6	
	δ_3,[a] mm/s	0.443	Fe^{3+} T_d	0.443	Fe^{3+} T_d	–		–		–	
	$\Delta E_{Q,3}$, mm/s	0.66		0.66		–		–		–	
	Γ_3, mm/s	0.592		0.592		–		–		–	
	A_3, %	24.5		5.1		–		–		–	
	δ_4,[a] mm/s	1.282	Fe^{2+}	1.382	Fe^{2+}	0.407	Fe^{3+} ox.	0.153	FeCo	0.139	FeCo
	$\Delta E_{Q,4}$, mm/s	3.13		2.93		–		–		–	
	H_4, T	–		–		51.2		37.2		36.7	
	Γ_4, mm/s	0.366		0.366		0.541		0.678		0.334	
	A_4, %	3.9		1.5		18.3		12.3		35.9	
	δ_5,[a] mm/s	–		0.500	Fe^{3+} SP	0.498	Fe^{3+} ox.	–		0.120	FeCo
	$\Delta E_{Q,5}$, mm/s	–		0.62		–		–		–	
	H_5, T	–		–		53.5		–		34.7	
	Γ_5, mm/s	–		1.115		0.402		–		0.299	
	A_5, %	–		28.3		63.4		–		37.1	

[a] Relative to room temperature α-iron foil

[b] If the relative areas do not sum up to 100%, there are unreported magnetic sextet contributions to the spectrum, see text

[c] The average values of two components

Table A2 Mössbauer spectral parameters for cloisite and sample **4a′**

T, K	Parameter	Na cloisite®	Assign.	Catalyst	Assign.	Calcined catalyst	Assign.	Composite	Assign.	CNT	Assign.
295	δ_1,[a] mm/s	0.373	Fe^{3+} *M*1	0.373	Fe^{3+} *M*1	0.378	Fe^{3+}	0.405	Fe^{3+}	0.306	Fe^{3+}
	$\Delta E_{Q,1}$, mm/s	1.24		1.24		1.97		0.81		0.703	
	Γ_1, mm/s	0.972		0.518		0.578		0.560		0.521	

Table A2 continued

T, K	Parameter	Na cloisite®	Assign.	Catalyst	Assign.	Calcined catalyst	Assign.	Composite	Assign.	CNT	Assign.
	A_1, %	20.7		9.1		9.0		30.6		6.5	
	δ_2,[a] mm/s	0.380	Fe^{3+} *M*2	0.380	Fe^{3+} *M*2	0.357	Fe^{3+}	1.036	Fe^{2+}	–	
	$\Delta E_{Q,2}$, mm/s	0.60		0.60		1.33		2.06		–	
	Γ_2, mm/s	0.891		0.475		0.499		0.605		–	
	A_2, %	41.4		18.2		11.5		64.6		–	
	δ_3,[a] mm/s	0.358	Fe^{3+} T_d	0.358	Fe^{3+} T_d	–		–		–	
	$\Delta E_{Q,3}$, mm/s	0.62		0.62		–		–		–	
	Γ_3, mm/s	0.592		0.316		–		–		–	
	A_3, %	33.2		14.6		–		–		–	
	δ_4,[a] mm/s	1.143	Fe^{2+}	–		0.312	Fe^{3+} ox.	–		0.025	FeCo[c]
	$\Delta E_{Q,4}$, mm/s	2.90		–		–		–		–	
	H_4, T	–		–		48.1		–		35.2	
	Γ_4, mm/s	0.366		–		0.890		–		0.352	
	A_4, %	4.6		–		29.1		–		93.5	
	δ_5,[a] mm/s	–		0.385	Fe^{3+} SP	0.374	Fe^{3+} ox.	0.18	Fe_3C	0.18	Fe_3C
	$\Delta E_{Q,5}$, mm/s	–		0.76		–		–		–	
	H_5, T	–		–		51.5		20.5		20.5	
	Γ_5, mm/s	–		0.540		0.283		0.350		0.452	
	A_5, %	–		58.2		50.5		4.7		4.1	
85[b]	δ_1,[a] mm/s	0.485	Fe^{3+} *M*1	0.485	Fe^{3+} *M*1	0.466	Fe^{3+}	0.468	$Fe^{3+,\ c}$	0.409	Fe^{3+}
	$\Delta E_{Q,1}$, mm/s	1.61		1.61		1.88		1.04		0.79	
	Γ_1, mm/s	0.972		0.972		0.668		0.651		0.473	
	A_1, %	15.3		7.1		11.9		21.0		6.3	
	δ_2,[a] mm/s	0.509	Fe^{3+} *M*2	0.509	Fe^{3+} *M*2	0.489	Fe^{3+}	1.179	$Fe^{2+,\ c}$	–	
	$\Delta E_{Q,2}$, mm/s	0.60		0.60		1.34		2.19		–	
	Γ_2, mm/s	0.891		0.891		0.480		0.531		–	
	A_2, %	30.6		14.2		8.7		61.4		–	
	δ_3,[a] mm/s	0.443	$Fe^{3+}T_d$	0.443	$Fe^{3+}T_d$	–		–		–	
	$\Delta E_{Q,3}$, mm/s	0.66		0.66		–		–		–	
	Γ_3, mm/s	0.592		0.592		–		–		–	
	A_3, %	24.5		12.1		–		–		–	
	δ_4,[a] mm/s	1.282	Fe^{2+}	–		0.386	Fe^{3+} ox.	0.142	FeCo	0.132	FeCo[c]
	$\Delta E_{Q,4}$, mm/s	3.13		–		–		–		–	
	H_4, T	–		–		50.9		36.1		36.0	
	Γ_4, mm/s	0.366		–		0.611		0.613		0.321	
	A_4, %	3.9		–		16.5		6.6		93.7	
	δ_5,[a] mm/s	–		0.500	Fe^{3+} SP	0.487	Fe^{3+} ox.	0.298	Fe_3C	0.298	Fe_3C
	$\Delta E_{Q,5}$, mm/s	–		0.56		–		–		–	
	H_5, T	–		–		53.7		24.5		24.5	
	Γ_5, mm/s	–		0.798		0.391		0.371		0.412	
	A_5, %	–		28.3		62.9		3.94		3.9	

[a] Relative to room temperature α-iron foil

[b] If the relative areas do not sum up to 100%, there are unreported magnetic sextet contributions to the spectrum, see text

[c] The average values of two components

Table A3 Mössbauer spectral parameters for cloisite and sample **4b′**

T, K	Parameter	Na cloisite®	Assign.	Catalyst	Assign.	Calcined catalyst	Assign.	Composite	Assign.	CNT	Assign.
295	δ_1, [a] mm/s	0.373	Fe^{3+} *M*1	0.373	Fe^{3+} *M*1	0.318	Fe^{3+}	0.376	Fe^{3+}	0.451	Fe^{3+}
	$\Delta E_{Q,1}$, mm/s	1.24		1.24		1.72		0.56		0.376	
	Γ_1, mm/s	0.972		0.543		0.687		0.379		0.547	
	A_1, %	20.7		9.0		35.0		9.8		31.6	
	δ_2,[a] mm/s	0.380	Fe^{3+} *M*2	0.380	Fe^{3+} *M*2	0.357	Fe^{3+}	0.997	Fe^{2+}	1.349	Fe^{2+}
	$\Delta E_{Q,2}$, mm/s	0.60		0.60		1.02		1.98		2.33	
	Γ_2, mm/s	0.891		0.497		0.691		0.464		0.442	
	A_2, %	41.4		18.0		65.0		9.1		68.4	
	δ_3,[a] mm/s	0.358	$Fe^{3+}T_d$	0.358	$Fe^{3+}T_d$	–		0.456	Fe^{3+}	–	
	$\Delta E_{Q,3}$, mm/s	0.62		0.62		–		0.98		–	
	Γ_3, mm/s	0.592		0.331		–		0.508		–	
	A_3, %	33.2		14.0		–		9.1		–	
	δ_4,[a] mm/s	1.143	Fe^{2+}	–		–		0.028	FeCo	–	
	$\Delta E_{Q,4}$, mm/s	2.90		–		–		–		–	
	H_4, T	–		–		–		35.2		–	
	Γ_4, mm/s	0.366		–		–		0.320[d]		–	
	A_4, %	4.6		–		–		58.8		–	
	δ_5,[a] mm/s	–		0.378	Fe^{3+} SP	–		1.068	Fe_2SiO_4	–	
	$\Delta E_{Q,5}$, mm/s	–		0.69		–		2.44		–	
	H_5, T	–		–		–		–		–	
	Γ_5, mm/s	–		0.482		–		0.451		–	
	A_5, %	–		59.0		–		12.1		–	
85[b]	δ_1,[a] mm/s	0.485	Fe^{3+} *M*1	0.485	Fe^{3+} *M*1	–		0.540	$Fe^{3+,\ c}$	0.501	Fe^{3+}
	$\Delta E_{Q,1}$, mm/s	1.61		1.61		–		0.85		0.532	
	Γ_1, mm/s	0.972		0.972		–		0.449		0.596	
	A_1, %	15.3		4.8		–		23.6		23.8	
	δ_2,[a] mm/s	0.509	Fe^{3+} *M*2	0.509	Fe^{3+} *M*2	0.443	Fe^{3+}	1.175	$Fe^{2+,\ c}$	1.447	Fe^{2+}
	$\Delta E_{Q,2}$, mm/s	0.60		0.60		1.39		2.34		3.33	
	Γ_2, mm/s	0.891		0.891		0.856		0.519		0.391	
	A_2, %	30.6		9.7		60.2		24.9		76.2	
	δ_3,[a] mm/s	0.443	$Fe^{3+}T_d$	0.443	$Fe^{3+}T_d$	–		–		–	
	$\Delta E_{Q,3}$, mm/s	0.66		0.66		–		–		–	
	Γ_3, mm/s	0.592		0.592		–		–		–	
	A_3, %	24.5		7.8		–		–		–	
	δ_4,[a] mm/s	1.282	Fe^{2+}	–	Fe^{2+}	0.490	Fe^{3+} ox.	0.142	FeCo	–	
	$\Delta E_{Q,4}$, mm/s	3.13		–		–		–		–	
	H_4, T	–		–		46.0		35.6		–	
	Γ_4, mm/s	0.366		–		0.696		0.361		–	
	A_4, %	3.9		–		19.9		59.3		–	
	δ_5,[a] mm/s	–		0.476	Fe^{3+} SP	0.458	Fe^{3+} ox.	–		–	
	$\Delta E_{Q,5}$, mm/s	–		0.66		–		–		–	
	H_5, T	–		–		50.4		–		–	
	Γ_5, mm/s	–		0.681		0.696		–		–	
	A_5, %	–		19.9		19.9		–		–	

[a] Relative to room temperature α-iron foil

[b] If the relative areas do not sum up to 100%, there are unreported magnetic sextet contributions to the spectrum, see text

[c] The average values of two components

[d] An incremental line width of 0.242 mm/s was used

References

1. Hernadi K, Fonseca A, Nagy JB, Bernaerts D, Lucas AA (1996) Carbon 34:1249
2. Hernadi K, Kónya Z, Siska A, Kiss J, Oszkó A, Nagy JB, Kiricsi I (2003) Mater Chem Phys 77:536
3. Hernadi K (2002) Chem Phys Lett 363:169
4. Gournis D, Karakassides MA, Bakas T, Boukos N, Petridis D (2003) Carbon 40:2641
5. Jankovic L, Gournis D, Dimos K, Karakassides MA, Bakas T (2005) J Phys Conf Series 10:178
6. Gil A, Gandia LM, Vicente MA (2000) Catal Rev Sci Eng 42:212
7. Endo M, Takeuchi K, Igarashi S, Kobori K, Shiraishi M, Kroto HW (1993) J Phys Chem Solids 54:1841
8. Pinnavaia TJ, Tzou MS, Landau SD, Raythatha RH (1984) J Mol Catal 27:195
9. Weaver CE, Pollard LD (1973) The chemistry of clay minerals developments in sedimentology, vol 15. Elsevier, New York, p 213
10. Bakandritsos A, Simopoulos A, Petridis D (2006) Nanotechnology 17:1112
11. Moore DM, Reynolds RC (1989) X-ray diffraction and the identification and analysis of clay minerals. Oxford University Press, Oxford, p 332
12. Thorez J (1976) Practical identification of clay minerals. A handbook for teachers and students in clay mineralogy. Lelotte, Dison, Belgium, p 90
13. Velde B (1992) Introduction to the clay minerals. Chapman and Hall, London, p 198
14. Önal M, Sarikaya Y, Alemdaroglu T, Bozdogan I (2003) Turk J Chem 27:683
15. Girgis BS, El Barawy KA, Felix NS (1987) Thermochim Acta 111:9
16. Van Bekkum H, Flanigen EM, Jacobs PA, Jansen JC (eds) (2001) Studies in surface science and catalysis, vol 137. Elsevier, Amsterdam
17. Storaro L, Lenarda M, Ganzerla R, Rinaldi A (1996) Microporous Mater 6:55
18. Ebbinghaus SG, Mauron PH, Reller A, Zhang Y, Zuttel A (2002) Mater Sci Eng C 19:119
19. Nagy JB, Bister G, Fonseca A, Méhn D, Konya Z, Kiricsi I, Horvath ZE, Biro LP (2004) J Nanosci Nanotech 4:326
20. Murad E, Johnston JH (1987) In: Long GJ (ed) Mössbauer spectroscopy applied to inorganic chemistry, vol 2. Plenum Press, New York, p 507
21. Coquay P, Vandenberghe RE, De Grave E, Fonseca A, Piedigrosso P, Nagy JB (2002) J Appl Phys 92:1286
22. Gangas NH, Simopoulos A, Kostikas A, Yassoglou NJ, Filippakis S (1973) Clays Clay Minerals 21:151
23. Rozenson I, Heller-Kallai L (1976) Clays Clay Minerals 24:271
24. Reis AS Jr, Ardisson JD (2003) Clays Clay Minerals 51:33
25. Coey JMD (1984) In: Long GJ (ed) Mössbauer spectroscopy applied to inorganic chemistry, vol 1. Plenum Press, New York, p 443
26. Badreddine R, Grandjean F, Vandormael D, Fransolet AM, Long GJ (2000) Clay Minerals 35:653
27. Methasiri T, Yoodee K, Tang IM (1980) Physica B 101:243
28. Tessonnier JP, Winé G, Estournès C, Leuvrey C, Ledoux MJ, Pham-Huu C (2005) Catal Today 102–103:29
29. Schuele WJ, Shtrikman S, Treves D (1965) J Appl Phys 36:1010
30. Skoutelas AP, Karakassides MA, Petridis D (1999) Chem Mater 11:2754
31. Bakandritsos A, Simopoulos A, Petridis D (2005) Chem Mater 17:3468
32. Pérez-Cabero M, Taboada JB, Guerrero-Ruiz A, Overweg AR, Rodriguez-Ramos I (2006) Phys Chem Chem Phys 8:1230
33. Johnson CE, Ridout MS, Cranshaw TE, Madsen PE (1961) Phys Rev Lett 6:450
34. Mancier V, Delplancke JL, Delwiche J, Hubin-Franskin MJ, Piquer C, Rebbouh L, Grandjean F (2004) J Magn Magn Mater 281:27
35. Delplancke JL, Dille J, Reisse J, Long GJ, Mohan A, Grandjean F (2000) Chem Mater 12:946
36. Dong XL, Zhang ZD, Jin SR, Kim BK (2000) J Magn Magn Mater 210:143
37. Da Silva Borchardt F (2004) Master's thesis, Univ Pittsburg, etd.library.pitt.edu/ETD/available/etd-10132004-194232
38. Kanetsuk Y, Ibaraki N, Ashida S (1991) ISIJ Int 31:304
39. Ruskov T, Asenov S, Spirov I, Garcia C, Mönch I, Graff A, Kozhuharova R, Leonhardt A, Mühl T, Ritschel M, Schneider C, Groudeva-Zotova S (2004) J Appl Phys 96:7514
40. Tokiro H, Fujii S, Muto S, Nasu S (2006) J Appl Phys 99:08Q512